Structural Engineering and Mechanics, *Vol. 70, No. 2 (2019) 179-197*
DOI: https://doi.org/10.12989/sem.2019.70.2.179

Geometry and load effects on transient response of a VFGM annular plate: An analytical approach

Seyed Hashem Alavi[a] and Hamidreza Eipakchi[*]

Faculty of Mechanical and Mechatronics Engineering, Shahrood University of Technology, P.O.Box 316, Shahrood, I.R. Iran

(Received November 1, 2018, Revised February 7, 2019, Accepted February 11, 2019)

Abstract. In this article, the effect of different geometrical, materials and load parameters on the transient response of axisymmetric viscoelastic functionally graded annular plates with different boundary conditions are studied. The behavior of the plate is assumed the elastic in bulk and viscoelastic in shear with the standard linear solid model. Also, the graded properties vary through the thickness according to a power law function. Three types of mostly applied transient loading, i.e., step, impulse, and harmonic with different load distribution respect to radius coordinate are examined. The motion equations and the corresponding boundary conditions are extracted by applying the first order shear deformation theory which are three coupled partial differential equations with variable coefficients. The resulting motion equations are solved analytically using the perturbation technique and the generalized Fourier series. The sensitivity of the response to the graded indexes, different transverse loads, aspect ratios, boundary conditions and the material properties are investigated too. The results are compared with the finite element analysis.

Keywords: annular plate; viscoelastic functionally graded materials; analytical solution; shear deformation theory; dynamic response

1. Introduction

The viscoelastic phenomenon is exhibited for a wide range of materials, including polymers, ceramics, metals, biological materials, geological materials, synthetic composites, and cellular solids. Due to the ability of these materials to energy loss, they are important in vibrations, sound control, dynamic stability, fatigue, and shock resistance. Furthermore, the functionally graded materials (FGM) which they are the materials with a non-homogeneous structure whose properties, such as density, Poisson's ratio, and Young's modulus vary continuously in one or two directions can be included by viscoelastic materials. Accordingly, the behavior investigation of the structures made up of viscoelastic functionally graded materials (VFGM) seems to be useful with more exact models due to development of technologies for producing such materials that have simultaneously vibration damping properties and continuity changes of the material properties. For the sake of difficulty and the high cost of experiments, the analytical approaches and simulations are of great significance. Consequently, different theoretical methods have been utilized by researchers to investigate the dynamic (Pawlus 2016), stress (Alipour and Shariyat 2013) and thermal (Rad and Shariyat 2016) behaviors of annular plates. Wang and Chen (2002) determined the natural frequencies and modal loss factors of a three-layered annular plate with two laminated face layers and a viscoelastic core using the finite elements method (FEM) through the first order shear deformation theory (FSDT). Salehi and Aghaei (2005) studied the dynamic large deflection of non-axisymmetric circular viscoelastic plates by employing the higher-order shear deformation theory and the finite difference technique. The standard linear solid (SLS) model was used for a viscoelastic material. Ansari et al. (2014) developed Mindlin's microplate model based on the modified strain gradient theory to determine the axisymmetric buckling, bending, and natural frequencies of circular and annular microplates composed of FG using the generalized differential quadrature (DQ) method. Liang *et al.* (2014, 2015) introduced a new method for response determination of the FGMs structures with the three-dimensional theory of elasticity. This method is a combination of the state space method, DQM, and numerical inverse Laplace transform. They investigated some different cases. They analyzed the annular plates with the various boundary conditions, the sector plates subjected to a transverse load with exponential distribution and different circular boundary conditions, a plate subjected to the underwater shock loading with considering the effect of fluid-solid interaction and the plate problem using the Kirchhoff thin plate theory under various boundary conditions. Dai *et al.* (2015) exhibited a transient response of a circular sandwich plate with an FG central disk and two piezoelectric layers based on the FSDT and geometrical nonlinear kinematic. The problem was solved by using the finite difference, Newmark's and iterative methods.

∗Corresponding author, Associate Professor
E-mail: hamidre_2000@yahoo.com
[a]M.Sc. Student
E-mail: sayed_hashem_alavi@yahoo.com

ISSN: 1225-4568 (Print), 1598-6217 (Online)

Khadem Moshir *et al.* (2017) declared an analytical procedure for free vibrations of annular viscoelastic plates based on the perturbation technique and the FSDT. Alavi and Eipakchi (2018) studied the asymmetric free vibrations behavior of an annular viscoelastic plate analytically by considering the FSDT formulation. Malekzadeh *et al.* (2018) used the FSDT and DQM for free vibration analysis of FG nanocomposite annular plate reinforces by graphene nanoplates.

According to the aforementioned survey of the literature, it seems that there are no studies to determine the dynamic response of VFGM annular plates under impulsive, step and harmonic transverse loads, different boundary conditions, and various load profiles with considering the structural damping, and FSDT analytically. Most researchers used the numerical methods such as the FEM to obtain the transient response of the FG plate. In the presented work, we tried to represent an analytical procedure to find the response of the annular VFGM plates based on the FSDT. In simulation of the viscoelastic structures, the most authors do not attend that the behavior of a viscoelastic structure is different in bulk (dilatational) and shear (deviatoric) and in the variety of viscoelastic structures, JUST the shear behavior is "viscoelastic" and it means that the shear modulus is time-dependent but they usually consider the tensile behavior as viscoelastic or Young`s modulus is time-dependent. Also, they usually derived the governing equation (which is usually "one" discrete equation) as a differential-integral form which it has an iterative (or numeric) solution. This research does not encounter this problem i.e. the shear and bulk behaviors are separated and an analytical solution based on the perturbation technique for the governing equations are presented which are three-coupled partial differential equations (PDE) with variable coefficients. In addition, several numerical cases are accomplished to study the effects of graded indexes, different transverse loads, aspect ratios, boundary conditions, and material properties such as the viscosity and elasticity modulus on the response of the VFGM plate. The results are compared with the FEM.

2. Basic formulation

2.1 Mechanical and geometrical characteristics

FGMs are often made up of a combination of two different materials, e.g., one metal and another ceramic in such a way that the properties of the resulting composition change as a continuous function of the spatial coordinates. In many applications, the importance of analyzing the dynamic behavior of structures made of FGM seems to be necessary. Therefore, the transient response characteristics are considered for FGM annular plates. For this purpose, an axisymmetric cylindrical coordinate system (r, z) with the origin at the center of the midplane (z=0) has been considered. In this system, r and z denote the radial and through-to-thickness directions, respectively. The plate has the outer radius r_o, inner radius r_i and thickness h. It is subjected to a transverse distributed pressure $Q(r,t)$ on the upper surface and t denotes the time. The geometric of the plate has been shown in Fig. 1. The material density and Young's modulus has been assumed to vary through the power law in the thickness direction. According to this rule, the mechanical characteristics of the VFGM plate such as, Young's modulus $E(z)$ and the mass density $\rho(z)$ has been supposed to vary as a function of the volume fractions that may be expressed in the following form (Srividhya *et al.* 2018)

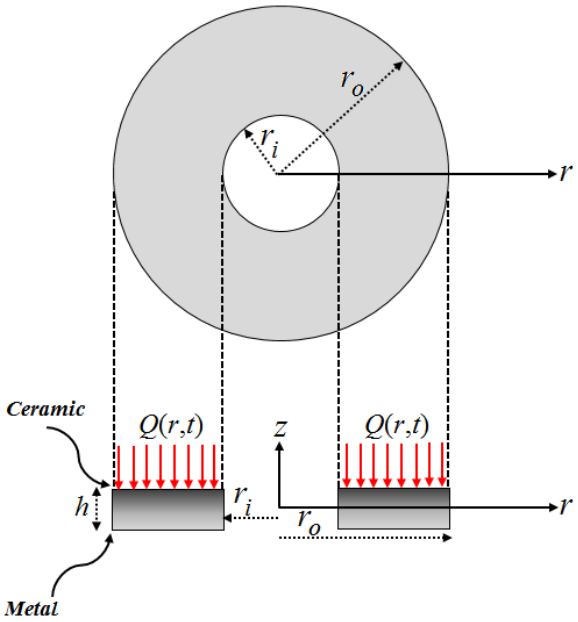

Fig. 1 Geometry of FG annular plate

$$E(z) = (E_c - E_m)V_f(z) + E_m$$
$$\rho(z) = (\rho_c - \rho_m)V_f(z) + \rho_m \quad (1a)$$

where E_c and E_m denote Young's modulus of the top and bottom materials, respectively; ρ_m and ρ_c indicate the mass density of materials at the bottom and top, respectively; V_f is the volume fraction of the material and it can be defined as follows (Srividhya e*t al.* 2018)

$$V_f(z) = (z/h + 0.5)^n \quad (1b)$$

n is the power-law index which takes positive values in this research and indicates the volume fraction gradation. Due to achieve a better describing of Eqs. (1), Young's modulus variation in the thickness direction z, for Al/Al_2O_3 annular plate with different values of grade index n, has been shown in Fig. 2. Based on Fig. 2, it is revealed that FG plate rapidly approaches to ceramic's one as $n<1$. Also, when $n>1$, the mixture of the metal phase is more than the ceramic one. It should be mentioned that, for n = 0 and n = ∞, the plate is totally ceramic and metal, respectively (which is not shown here).

2.2 Governing equations

Based on the FSDT, for an axisymmetric case, the radial

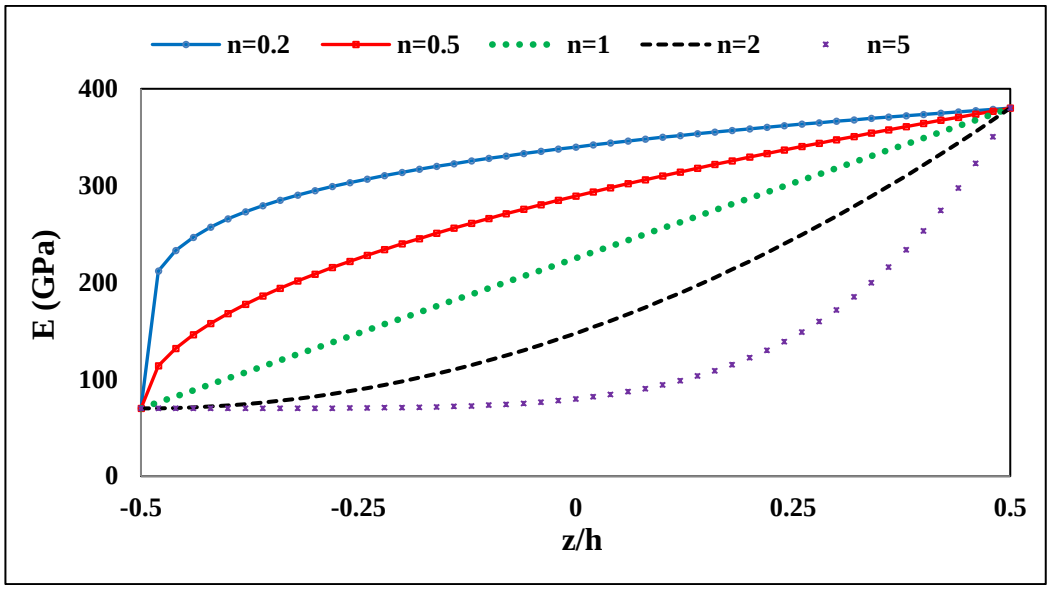

Fig. 2 Variation of Young modulus for various value of grade index through the dimensionless thickness

and transverse displacement components $u(r,z,t)$ and $w(r,z,t)$ for a point in the annular FG plate are written as follows

$$u(r,z,t) = u_0(r,t) + zu_1(r,t)$$
$$w(r,z,t) = w_0(r,t) \tag{2}$$

in which, u_0, w_0 denote the radial and transverse displacements of the mid-plane and u_1 is an unknown dimensionless function. The strain-displacement relations for axisymmetric small deformations can be written as the following (Sadd 2009)

$$\varepsilon_r = \frac{\partial u}{\partial r} = \frac{\partial u_0}{\partial r} + z\frac{\partial u_1}{\partial r};\ \varepsilon_z = \frac{\partial w}{\partial z} = 0$$
$$\varepsilon_\theta = \frac{u}{r} + \frac{1}{r}\frac{\partial v}{\partial \theta} = \frac{1}{r}(u_0 + zu_1); \tag{3}$$
$$\gamma_{rz} = \frac{\partial w}{\partial r} + \frac{\partial u}{\partial z} = \frac{\partial w_0}{\partial r} + u_1$$

The stress-strain relations, according to the Hooke law can be represented as (Sadd 2009)

$$\sigma_r = (K - \frac{2G}{3})(\varepsilon_r + \varepsilon_\theta + \varepsilon_z) + 2G\varepsilon_r$$
$$\sigma_\theta = (K - \frac{2G}{3})(\varepsilon_r + \varepsilon_\theta + \varepsilon_z) + 2G\varepsilon_\theta \tag{4}$$
$$\sigma_z = (K - \frac{2G}{3})(\varepsilon_r + \varepsilon_\theta + \varepsilon_z) + 2G\varepsilon_z; \tau_{rz} = G\gamma_{rz}$$

where K, G are the bulk and shear modulus. The kinetic energy T and the strain energy U of an *elastic* plate may be expressed as

$$T = \pi\int_{r_i}^{r_o}\int_{-h/2}^{h/2}\rho(z)(\dot{u}^2 + \dot{w}^2)rdrdz$$
$$U = \pi\int_{r_i}^{r_o}\int_{-h/2}^{h/2}(\sigma_r\varepsilon_r + \sigma_\theta\varepsilon_\theta + \tau_{rz}\gamma_{rz})rdrdz \tag{5a}$$

The external work due to the transverse distributed pressure Q which is applied on the upper surface of the plate ($z=h/2$) can be defined as follows

$$W_Q = \int_{r_i}^{r_o}\int_0^{2\pi} r\,Q(r,t)\,w(r,h/2,t)\,drd\theta \tag{5b}$$

By using Hamilton's principle, the governing equations and the boundary conditions are derived (Sadd 2009).

$$\delta\int_{t_1}^{t_2} Ldt = 0; L = T - U + W_Q \tag{6}$$

On the basis of Eqs. (5), (6), three equations of motion in terms of the stress resultants are determined as the following

$$-rI_0\ddot{u}_0 + (rN_r)_{,r} - N_\theta = 0$$
$$-rI_2\ddot{u}_1 + (rM_r)_{,r} - M_\theta - rQ_r = 0 \tag{7a}$$
$$-rI_0\ddot{w}_0 + (rQ_r)_{,r} = -rQ(r,t)$$

where the superscript dot denotes the partial derivative with respect to time. The stress resultants and the inertia terms are defined as follows

$$(N_r, N_\theta, Q_r) = \int_{-h/2}^{h/2}(\sigma_r, \sigma_\theta, K_s\tau_{rz})dz$$
$$(M_r, M_\theta, M_{rz}) = \int_{-h/2}^{h/2} z(\sigma_r, \sigma_\theta, K_s\tau_{rz})dz \tag{7b}$$
$$I_i = \int_{-h/2}^{h/2}\rho z^i dz \qquad (i = 0, 2)$$

K_s denotes the shear correction factor. It is well-known that the first-order shear deformation plate theory requires an appropriate shear correction factor to compute the transverse shear force. This quantity depends on some factors e.g., the shape of the cross-section, Poisson's ratio, and aspect ratio. Some researchers presented the formulas

to calculate this parameter (Faghidian 2017, Romano *et al.* 2015). The presented formula in different papers usually relates to the homogenous structures. In the current investigation, the structure has the time-dependent and FG properties simultaneously and here, an average value K_s=5/6 is accepted (Shariyat and Alipour 2013). The boundary conditions corresponding to Eq. (7a) for an annular plate is

$$[rN_r\delta u_0]_{r_i}^{r_o}=0;\ [rM_r\delta u_1]_{r_i}^{r_o}=0;\ [rQ_r\delta w_0]_{r_i}^{r_o}=0 \quad (7c)$$

In order to derive the governing equations, it is necessary to choose a rheological model. These models contain different combinations of spring and dashpot elements. Three custom models are Maxwell, Kelvin, and SLS models (Fig. 3). The investigation of their constitutive equations shows that the Maxwell model cannot predict the creep behavior of a viscoelastic material and the Kevin model is not appropriate to model the relaxation behavior but the SLS model is successful to describe both the relaxation and creep behaviors. (Brinson and Brinso 2008). So, in the presented study, the SLS model is used for the formulation of the problem. Also, it is assumed that the viscoelastic material obeys the SLS model in shear and elastic in bulk i.e., K=K_0 where K_0 is a constant (elastic bulk modulus). The general state of the stress at a point can be separated into two parts, one relates to a change of shape (deviatoric) and the other return to the change of volume (dilatational). For the deviatoric part, one can write $P_1\tau_{ij}$=$Q_1\gamma_{ij}$. P_1, Q_1 are differential operators and include the modulus and viscosity of each spring and damper in the mechanical models. In the elastic case, the shear stress-strain relation is τ_{ij}=$2G\varepsilon_{ij}$, so G=$Q_1/2P_1$. The viscoelastic operators are expressed as the following (Brinson and Brinson 2008)

$$\begin{aligned} &Q_1=2(1+\tau D);\ P_1=(\frac{1}{G_1}+\frac{1}{G_2})+\frac{\tau}{G_1}D \\ &\tau=\frac{\eta}{G_2};\ D=\frac{\partial}{\partial t};\ G_0^*=K(\frac{1}{G_1}+\frac{1}{G_2});\ G_1^*=\frac{K}{G_1} \end{aligned} \quad (8)$$

where τ is the relaxation time and D is the time derivative operator. By substituting G into Eq. (7a) and applying the time derivative operator on the equations, the governing differential equations of motion for a VFGM plate are derived in the general following form

$$\begin{aligned} &L_i[u_0,w_0,u_1,r,t,\partial^{n+m}/\partial t^n\partial r^m,Q(r,t)]=0 \\ &m=0..2,\ \ n=0..3, i=1..3 \end{aligned} \quad (9)$$

L_i are differential operators and Eqs. (9) contain three coupled partial differential equations with varying coefficients.

3. Analytical solution

For generality and convenience, the motion equations are converted to non-dimensional forms at first and the perturbation technique is utilized to solve them. The non-

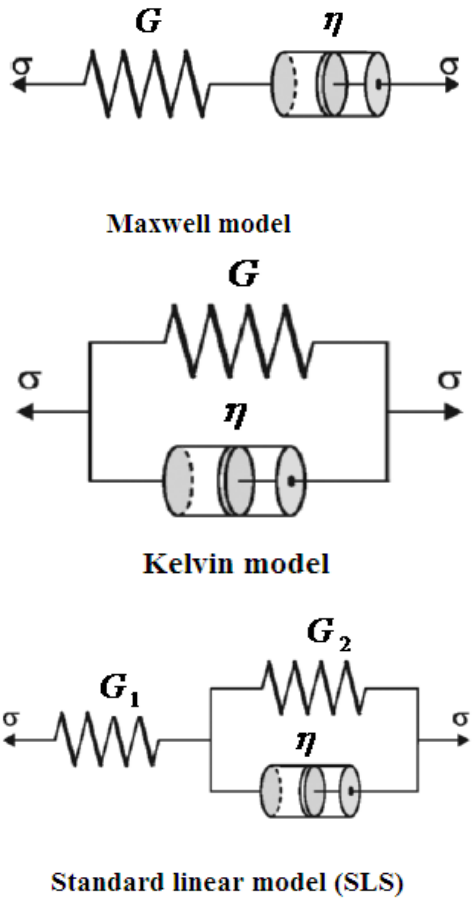

Fig. 3 Rheological models (Brinson and Brinson 2008)

dimensional terms are introduced as follows

$$r^*=\frac{r}{r_0};t^*=\frac{t}{t_0};u_0^*=\frac{u_0}{h};u_1^*=u_1;w_0^*=\frac{w_0}{h} \quad (10a)$$

where $(..)^*$ stands of the non-dimensional form of the quantity (..). By applying Eqs. (10a) into governing equations Eqs. (9), the following non-dimensional terms appear as the coefficients of some terms

$$e=\frac{\rho h^2}{K_0t_0^2};\beta=\frac{\tau}{t_0};\varepsilon=\frac{h}{r_0};t_0=\frac{r_0}{\sqrt{K_0/\rho}} \quad (10b)$$

ε is a small parameter which is taken as the perturbation parameter. Also, a new space variable X=(r^*-1)/ε is defined. The method of multiple scales in perturbation technique is used for the solution. The used timescales are T_0=t^*, T_1=ε t^* (Nayfe 1993). Using the chain rule implies

$$\begin{aligned} &\frac{\partial}{\partial t^*}=\frac{\partial}{\partial T_0}+\varepsilon\frac{\partial}{\partial T_1};\frac{\partial^2}{\partial t^{*2}}=\frac{\partial^2}{\partial T_0^2}+2\varepsilon\frac{\partial^2}{\partial T_0\partial T_1} \\ &\frac{\partial^3}{\partial t^{*3}}=\frac{\partial^3}{\partial T_0^3}+3\varepsilon\frac{\partial^3}{\partial T_0^2\partial T_1} \end{aligned} \quad (11)$$

By substituting Eqs. (10), (11) into Eq. (9), the non-dimensional forms of motion equations are obtained as follows

$$Eq_1: L_{10}[u_0^*, u_1^*] + \varepsilon L_{11}[u_0^*, u_1^*] + \varepsilon^2 R_{12}[u_0^*, u_1^*, \varepsilon] = 0 \tag{12a}$$

$$Eq_2: L_{20}[u_0^*, u_1^*, w_0^*] + \varepsilon L_{21}[u_0^*, u_1^*, w_0^*] + \varepsilon^2 R_{22}[u_0^*, u_1^*, w_0^*, \varepsilon] = 0 \tag{12b}$$

$$Eq_3: L_{30}[u_1^*, w_0^*, Q^*] + \varepsilon L_{31}[u_1^*, w_0^*, Q^*] + \varepsilon^2 R_{32}[u_1^*, w_0^*, \varepsilon] = 0 \tag{12c}$$

L and R are differential operators. The explicit dimensionless forms of operators are given in the appendix. It should be noted that Eq. (12c) is a none-homogeneous equation. Here, an analytical approach based on the perturbation method for the response of the presented VFGM plate is applied. We seek a straightforward expansion for the solution as the following

$$\begin{aligned} u_0^*(X, t^*; \varepsilon) &= u_{00}^*(X, T_0, T_1) + \varepsilon u_{01}^*(X, T_0, T_1) \\ u_1^*(X, t^*; \varepsilon) &= u_{10}^*(X, T_0, T_1) + \varepsilon u_{11}^*(X, T_0, T_1) \\ w_0^*(X, t^*; \varepsilon) &= w_{00}^*(X, T_0, T_1) + \varepsilon w_{01}^*(X, T_0, T_1) \end{aligned} \tag{13}$$

The equations for different orders of ε can be specified as follows

$$O(\varepsilon^0): \quad Eq_1: L_{10}[u_{00}^*, u_{10}^*] = 0; Eq_2: L_{20}[u_{00}^*, u_{10}^*, w_{00}^*] = 0 \quad Eq_3: L_{30}[u_{10}^*, w_{00}^*, Q^*] = 0 \tag{14a}$$

$$O(\varepsilon): \quad \begin{aligned} Eq_1 &: L_{10}[u_{01}^*, u_{11}^*] + L_{11}[u_{00}^*, u_{10}^*] = 0 \\ Eq_2 &: L_{20}[u_{01}^*, u_{11}^*, w_{01}^*] + L_{21}[u_{00}^*, u_{10}^*, w_{00}^*] = 0 \\ Eq_3 &: L_{30}[u_{11}^*, w_{01}^*, Q^*] + L_{31}[u_{10}^*, w_{00}^*, Q^*] = 0 \end{aligned} \tag{14b}$$

Eqs. (14) are non-homogeneous systems of coupled partial differential equations with constant coefficients. According to Eq. (7c), the boundary conditions for special cases are defined as the following

$$\text{Clamped:} \quad u_0 = 0; u_1 = 0; w_0 = 0 \tag{14c}$$

$$\text{Simply supported:} \quad rM_r = 0; u_0 = 0; w_0 = 0 \tag{14d}$$

$$\text{Free:} \quad rN_r = 0; rM_r = 0; rQ_r = 0 \tag{14e}$$

3.1 Order-zero

The solution of Eqs. (14a) in agreement with the generalized Fourier series method may be represented as

$$\begin{aligned} u_{00}^*(X, T_0, T_1) &= \sum_{m=1}^{\infty} A_{1m}(T_0, T_1)\varphi_{1m}(X) \\ u_{10}^*(X, T_0, T_1) &= \sum_{m=1}^{\infty} A_{2m}(T_0, T_1)\varphi_{2m}(X) \\ w_{00}^*(X, T_0, T_1) &= \sum_{m=1}^{\infty} A_{3m}(T_0, T_1)\varphi_{3m}(X) \end{aligned} \tag{15}$$

where $L=X_o-X_i$ and φ_{im} (i=1..3) are the mode shapes (eigenfunctions) of the system which are extracted by solving the homogenous form of Eq. (14a) employing the perturbation technique (Khadem *et al.* 2017, Alavi and Eipakchi 2018). By substituting Eqs. (15) into Eq. (14a), it results that

$$\sum_{m=1}^{\infty} P_{1m}\varphi_{1m}(X) = F_1; \sum_{m=1}^{\infty} P_{2m}\varphi_{2m}(X) = F_2 \quad \sum_{m=1}^{\infty} P_{3m}\varphi_{3m}(X) = F_3 \tag{16}$$

Because there are different equations for each value of the graded index, we present the formulas just for n=1

$$\begin{aligned} P_{1m} &= -18\lambda^2 a_0(\mu_1 + 1)g_3[A_{1m}] + \\ &3\lambda^2 a_0(1-\mu_1)g_3[A_{2m}] - 18e(\mu_2 + 1)g_5[A_{1m}]; \\ &\lambda = m\pi / L; \mu_1 = E_c / E_m; \\ &\mu_2 = \rho_c / \rho_m; a_0 = G_0^* + 4/3 \end{aligned} \tag{17a}$$

$$\begin{aligned} P_{2m} &= 6\lambda^2 a_0(1-\mu_1)g_3[A_{1m}] - \\ &(3\lambda^2 a_0 + 36K_s)(1+\mu_1)g_3[A_{2m}] - \\ &3e(\mu_2 + 1)g_5[A_{2m}] - 36K_s\lambda(1+\mu_1)g_3[A_{5m}] \end{aligned} \tag{17b}$$

$$\begin{aligned} P_{3m} &= -K_s\lambda(1+\mu_1)g_3[A_{2m}] - \\ &K_s\lambda^2(1+\mu_1)g_3[A_{5m}] - e(\mu_2 + 1)g_5[A_{5m}]; \\ &F_1 = 0; F_2 = 0; F_3 = \zeta g_4[Q^*] \end{aligned} \tag{17c}$$

P_{1m}, P_{2m}, and P_{3m} are calculated from the orthogonality property as follows

$$P_{jm} = \frac{(F_j, \varphi_{jm}(X))}{(\varphi_{jm}(X), \varphi_{jm}(X))} \tag{18a}$$

where (p,q) is the inner product of the functions and it is defined as follows

$$(p(X), q(X)) = \int_{X_i}^{X_o} p(X).q(X)\, dX \tag{18b}$$

Eqs. (17) are three coupled ordinary differential equations which their general solutions can be considered as

$$A_{1m}(T_0,T_1)=\sum_{j=1}^{9}a_j(T_1)e^{i\alpha_j T_0}$$

$$A_{2m}(T_0,T_1)=\sum_{j=1}^{9}b_j(T_1)e^{i\alpha_j T_0} \quad (19)$$

$$A_{3m}(T_0,T_1)=\sum_{j=1}^{9}c_j(T_1)e^{i\alpha_j T_0}$$

α_j (j=1..9) are eigenvalues of Eqs. (17). $a_j(T_1)$, $b_j(T_1)$ and $c_j(T_1)$ are unknown coefficients that will be determined later.

3.2 Order-one

The solutions of Eq. (14b) are considered as the following

$$u_{01}^{*}(X,T_0,T_1)=\sum_{m=1}^{\infty}B_{1m}(T_0,T_1)\varphi_{1m}(X)$$
$$u_{11}^{*}(X,T_0,T_1)=\sum_{m=1}^{\infty}B_{2m}(T_0,T_1)\varphi_{2m}(X) \quad (20)$$
$$w_{01}^{*}(X,T_0,T_1)=\sum_{m=1}^{\infty}B_{3m}(T_0,T_1)\varphi_{3m}(X)$$

By using Eqs. (20), (15), (14b) it results that

$$\sum_{m=1}^{\infty}K_{1m}\varphi_{1m}(X)=F_1;\sum_{m=1}^{\infty}K_{2m}\varphi_{2m}(X)=F_2$$
$$\sum_{m=1}^{\infty}K_{3m}\varphi_{3m}(X)=F_3 \quad (21)$$

where

$$K_{jm}=\frac{(F_j,\varphi_{jm}(X))}{(\varphi_{jm}(X),\varphi_{jm}(X))} \quad (22)$$

On the basis of Eq. (22), it is known that Eqs. (14b) have secular terms and before determination its particular solution, it requires to eliminate its secularity. For this object, the solvability condition is employed (Nayfeh 1993). The particular solutions of Eq. (22) for secular terms can be written

$$B_{1m}(T_0,T_1)=\sum_{j=1}^{9}P_{22j}(T_1)e^{i\alpha_j T_0}$$

$$B_{2m}(T_0,T_1)=\sum_{j=1}^{9}R_{22j}(T_1)e^{i\alpha_j T_0} \quad (23)$$

$$B_{3m}(T_0,T_1)=\sum_{j=1}^{9}Q_{22j}(T_1)e^{i\alpha_j T_0}$$

By substituting Eqs. (23) into Eqs. (22), and picking out the terms with coefficients $exp\ (i\alpha_j T_0)$ (j=1..9), a set of first order ordinary differential equations to assess $\alpha_j(T_1)$, $b_j(T_1)$ and $c_j(T_1)$ is detected. The constants composed in solving differential equations can be computed by employing the zero initial conditions.

Table 1 Geometrical and material properties

Outer radius (m)	$a=r_o$=0.15
Viscoelastic modulus (MPa)	G_1=0.55, G_2=9.5
Viscosity coefficient (Pa.s)	η=7.6E4
Ceramic density (Al_2O_3) (Kg/m^3)	ρ_c= 3800
Metal density (Al) (Kg/m^3)	ρ_m=2070
Ceramic modulus (GPa)	E_c = 380
Metal modulus (GPa)	E_m = 70
Poisson's ratio	ν=0.3

Table 2 Equations of different load distribution

Profile	Equation: Q(X)=Q$_0$.f(X)	
Constant	f(X)=1	-
Linear	f(X)= a_1X + b_1	a_1=6.473×10^{-5}, b_1=4.531×10^{-4}
Parabolic	f(X)= a_1X^2 + b_1X	a_1= -2.774×10^{-5}, b_1= -1.942×10^{-4}
Sine	f(X)= $a_1$sin(πX/L); L=X_{out} - X_{in}	a_1= -3.559×10^{-4}

4. Numerical analysis

Before exhibiting the results, the efficiency of the proposed solution technique should be examined. Abaqus *FE* package has been utilized for numerical analysis. CAX8R element has been used in this study which is a quadratic axisymmetric element with eight nodes and two translation degrees of freedom in each node. The viscoelastic shear modulus is defined using the Prony series as the following

$$G_R(t)=G_{00}\left(1-\sum_{i=1}^{N}q_i^G(1-e^{-\frac{t}{\tau_i^G}})\right)$$
$$q_i^G=\frac{G_i}{G_{00}};\tau_i^G=\frac{\eta}{G_1+G_2};G_i=\frac{G_1^2}{G_1+G_2} \quad (24a)$$

In this research for the SLS model, values N=1, G_{00}=G_1 were adopted. After modeling the viscoelastic behavior, the user-defined field (USDFLD) technique was used to apply the material properties changes through the thickness direction based on the power law distribution (Abaqus User Manual 2013). Also a sensitivity analysis has been performed for determining the mesh size and time step. The characteristics of the structure have been listed in Table 1.

The results obtained for the viscoelastic plate can be obtained by substituting $\tau\rightarrow 0$ to an elastic plate. For this case, Fig. 3 is converted to two parallel springs which have the equivalent value G_s as the following

$$G_s=\frac{G_1G_2}{G_1+G_2} \quad for\ \eta=0 \quad (24b)$$

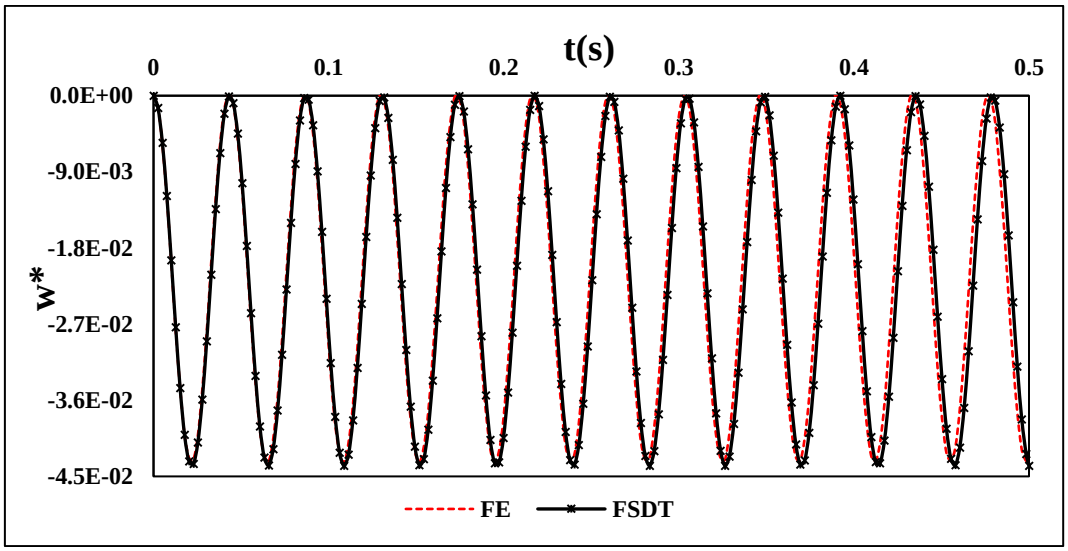

Fig. 4 Analytical and numerical transverse response

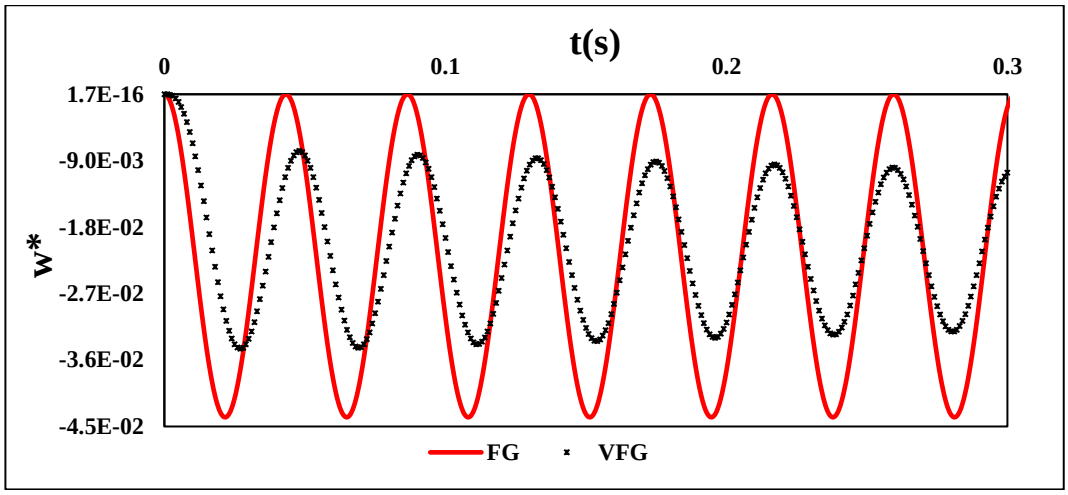

Fig. 5(a) Effect of viscoelasticity on dynamic response of FG and VFGM plate (S-S)

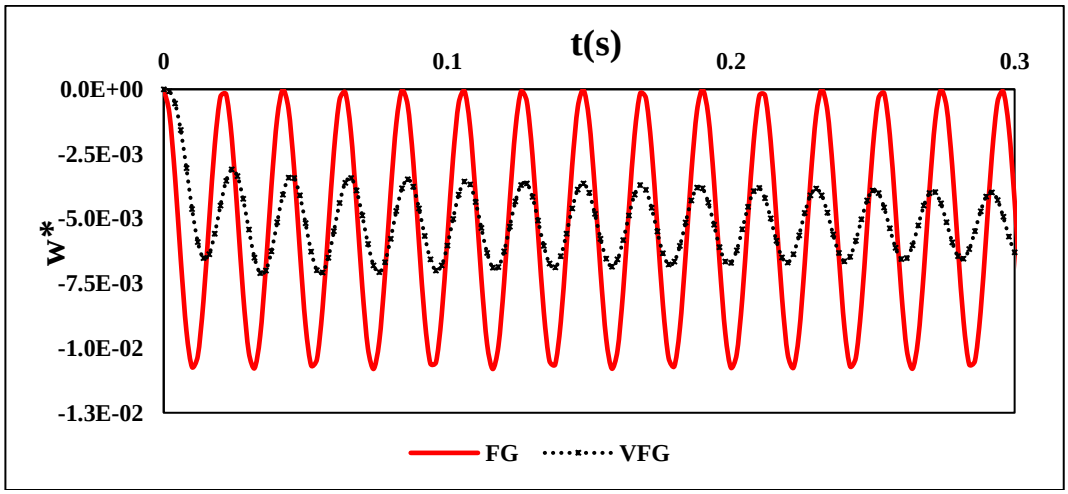

Fig. 5(b) Effect of viscoelasticity on dynamic response of FG and VFGM plate (C-C)

For high damping ($\eta\to\infty$) the equivalent shear modulus is $G_s= G_1$. For the values $\eta\neq0$, the equivalent shear modulus has been defined as $G_s=G_1$ in this research. The bulk modulus K_0, is as the following

$$K_0 = \frac{2}{3} G_s \frac{1+\nu}{1-2\nu} \tag{24c}$$

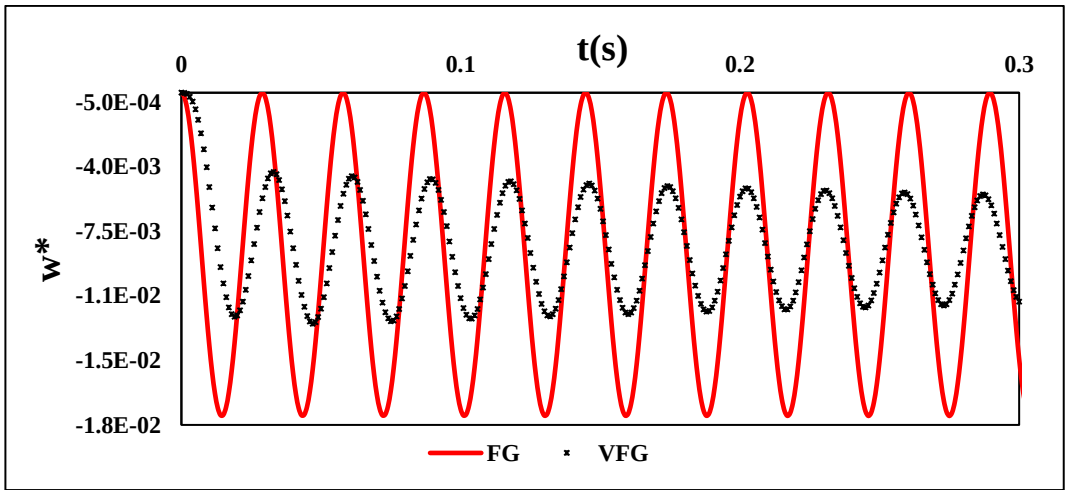

Fig. 5(c) Effect of viscoelasticity on dynamic response of FG and VFGM plate (S-C)

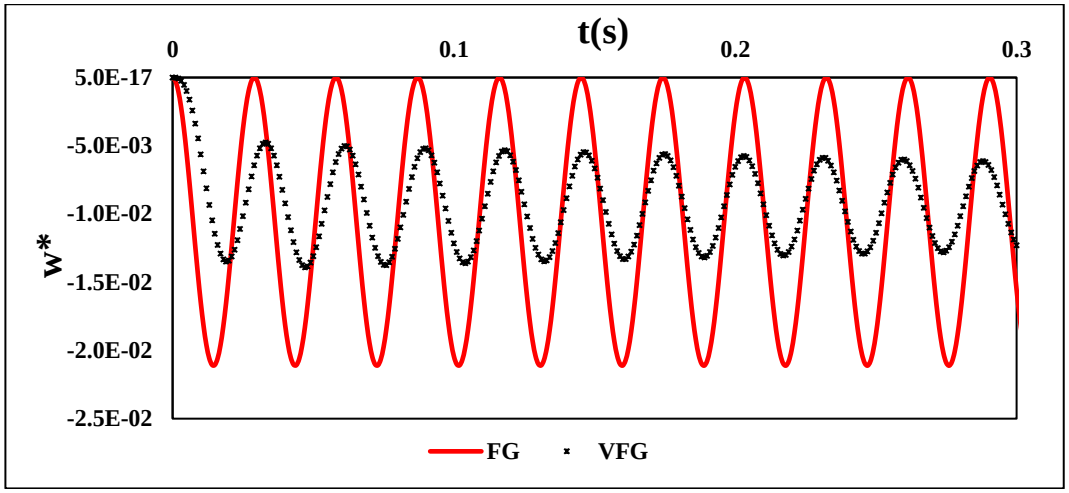

Fig. 5(d) Effect of viscoelasticity on dynamic response of FG and VFGM plate (C-S)

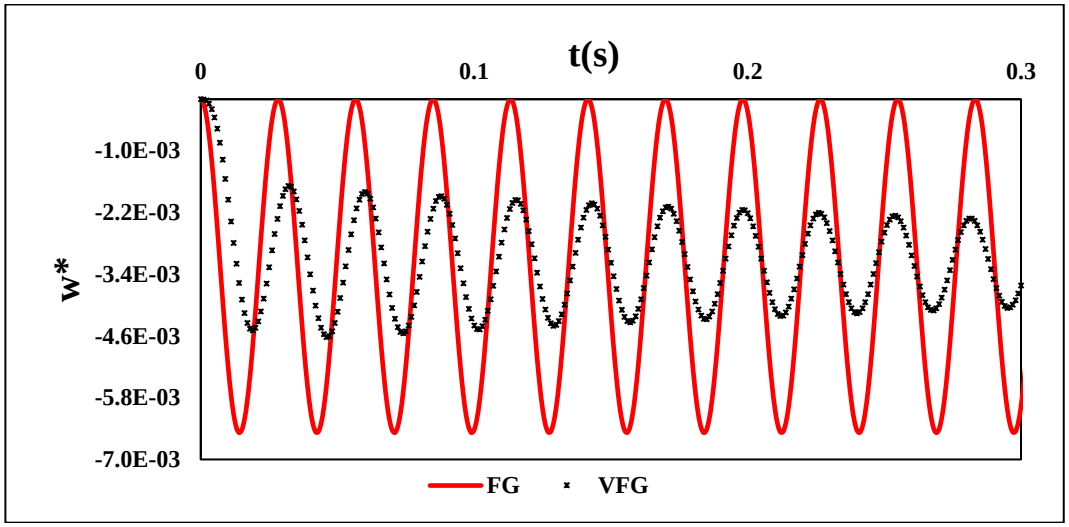

Fig. 5(e) Effect of viscoelasticity on dynamic response of FG and VFGM plate (S-F)

K_0 is used in Eqs. (10) and it is just to report the results as dimensionless quantities.

5. Results and discussion

A mathematical program was developed to find the dynamic response of a VFGM plate based on the presented

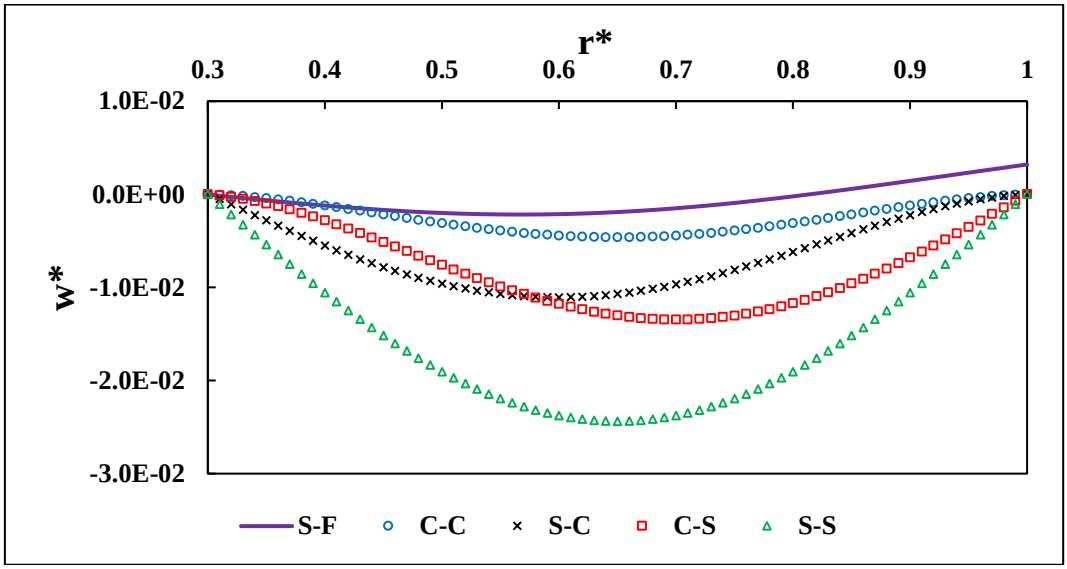

Fig. 6 Transverse deflection for different boundary conditions t = 0.5 s

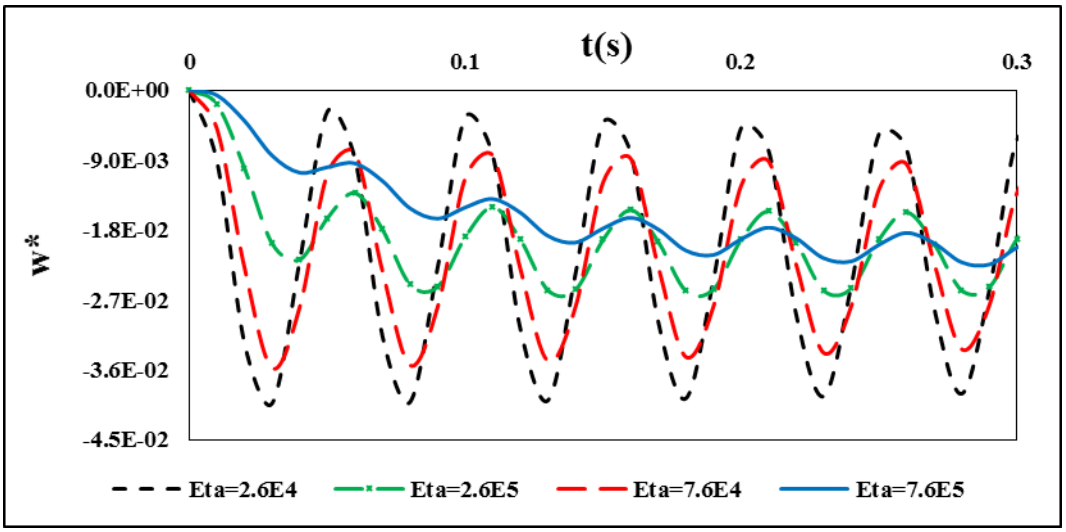

Fig. 7 Transverse response for different viscoelastic coefficients (η-Pa.s)

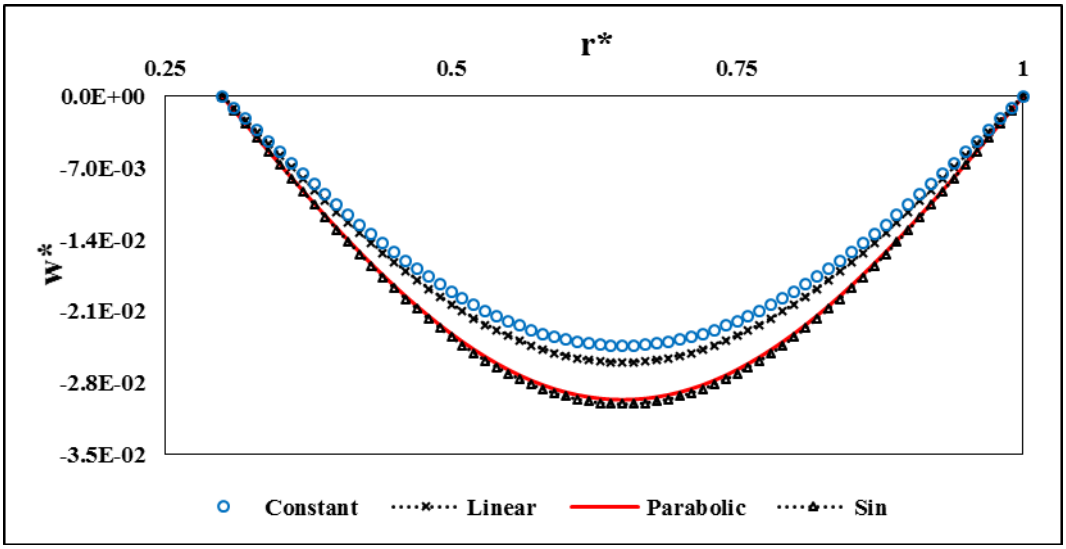

Fig. 8 Transverse deflection for different load profiles t = 0.5 s

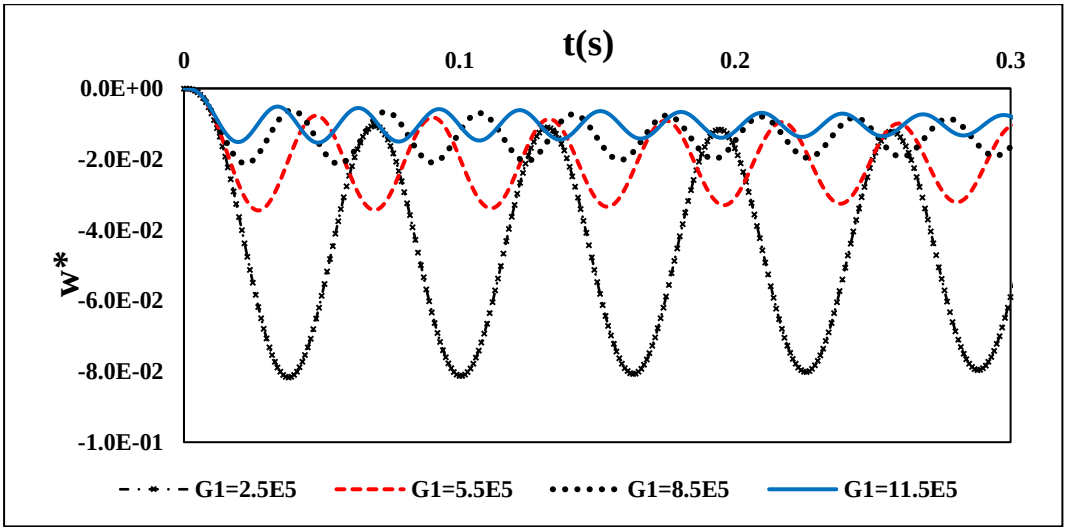

Fig. 9(a) Transverse response for different elasticity modulus (G1- Pa)

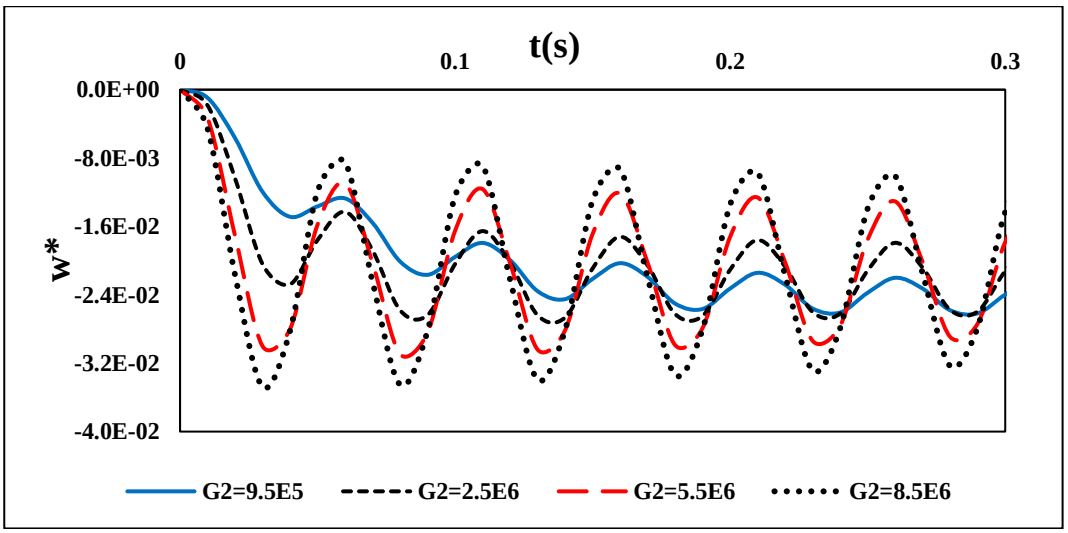

Fig. 9(b) Transverse response for different elasticity modulus (G2-Pa)

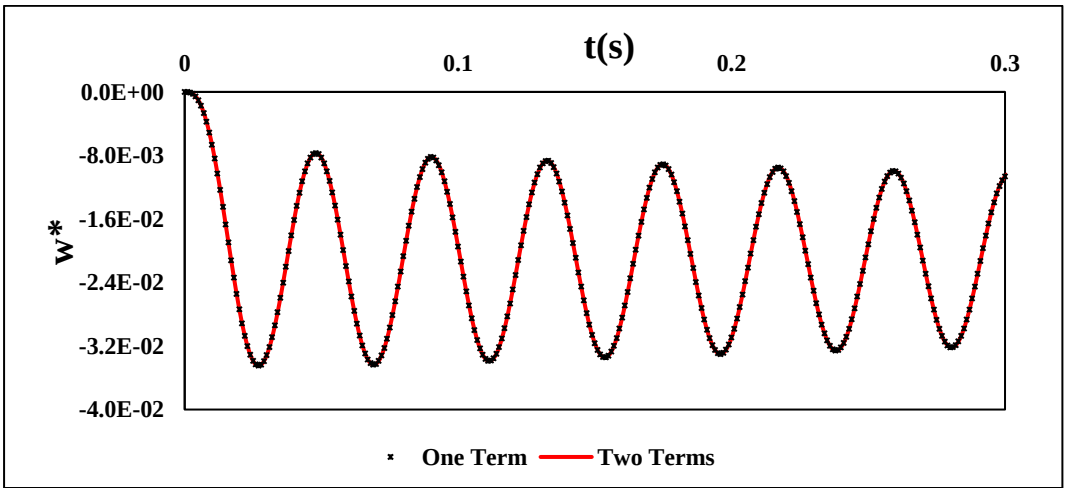

Fig. 10 Transverse response for one and two terms

analytical solution on Maple 15 environment. The effects of the main parameters such as load type, boundary conditions, thickness ratio *hr=h/a*, aspect ratio *rr=ri/ro*, viscose coefficient, elasticity modulus, and grade index on the

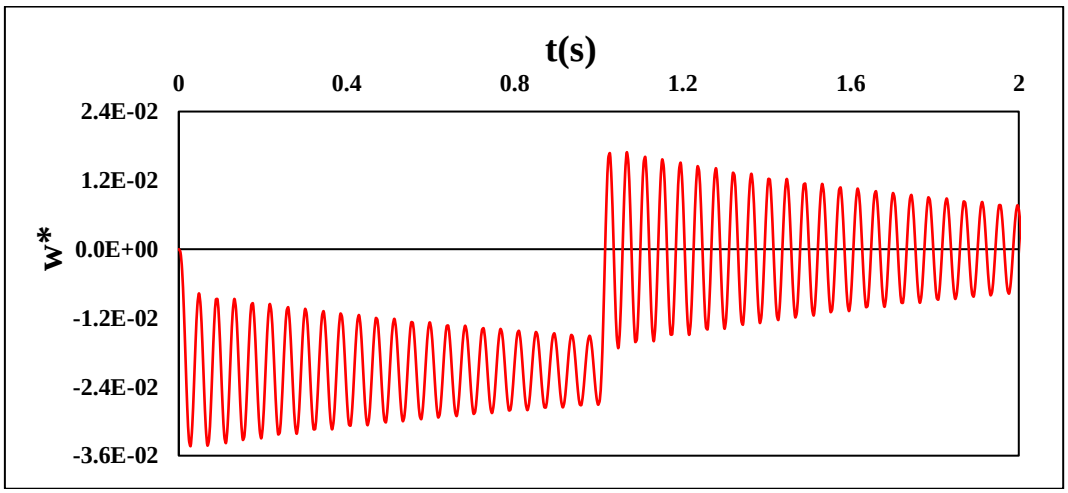

Fig. 11 Transverse response for step function loading

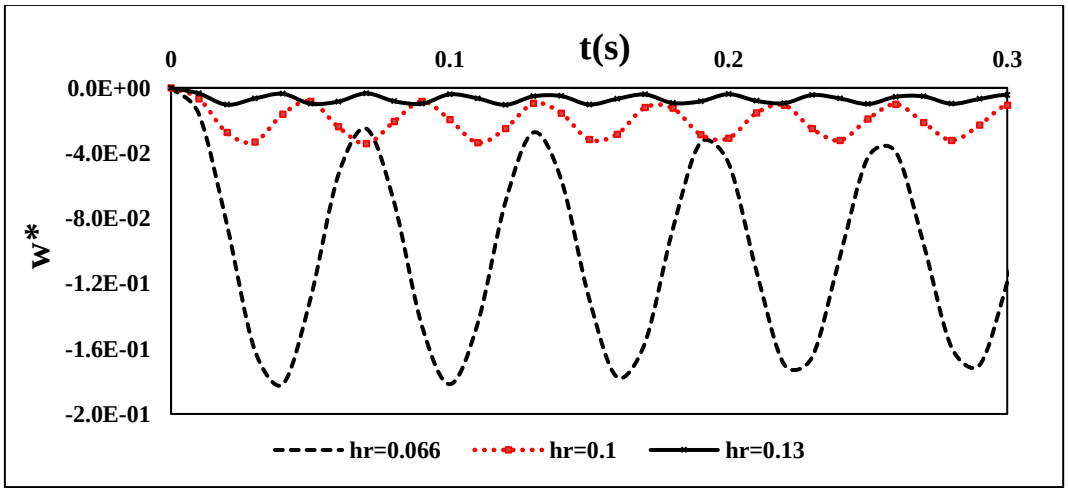

Fig. 12(a) Transverse response for different thickness ratio

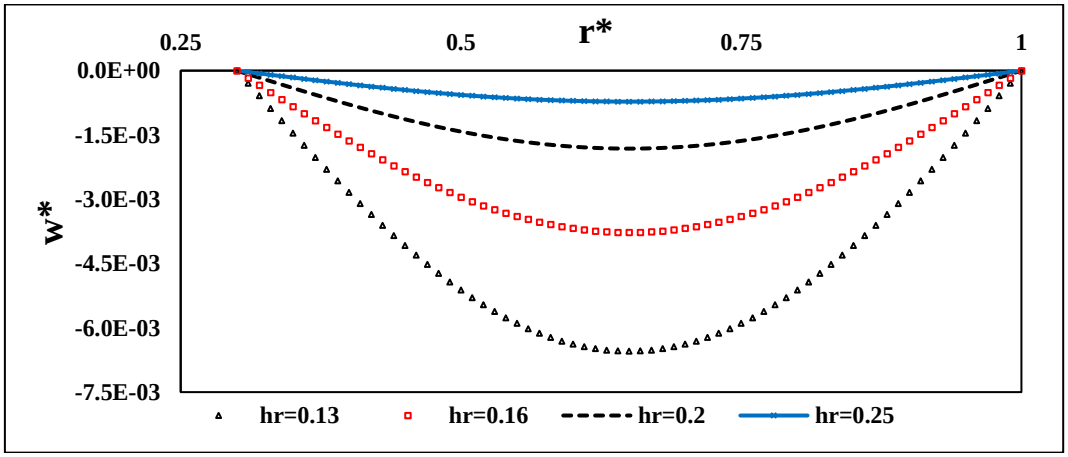

Fig. 12(b) Transverse deflection for different thickness ratio

dynamic response behaviors of VFGM annular plates are examined. An FE analysis using Abaqus package has been employed as a benchmark to demonstrate the correctness of the presented method. The optimum element number was 1800 and the time step was adopted as 0.001 sec by trial and error. All the time responses have been reported for the FSDT, at $r=(ro+ri)/2$ (mid-radius), $hr=0.1$, $rr=0.3$, $n=1$, constant load profile and simply supported except that the mentioned cases.

5.1 Transient response under step function

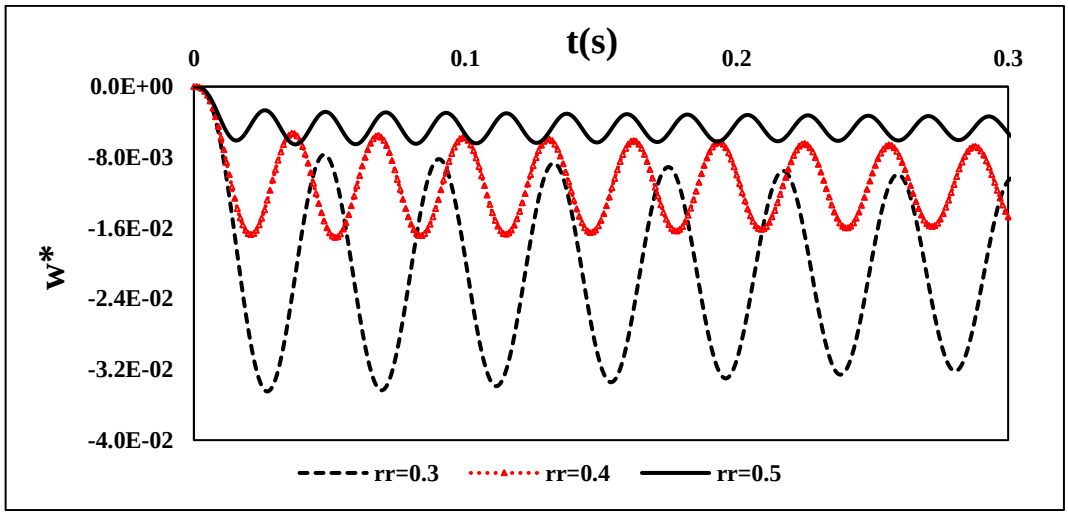

Fig. 13 Transverse response for different radius ratio

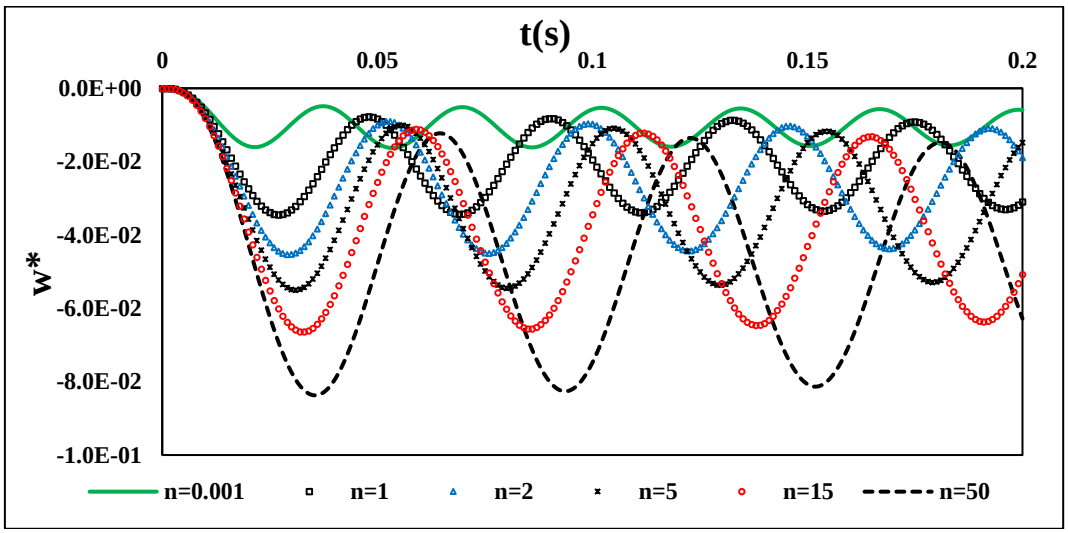

Fig. 14 Effect of volume fraction (n) on response of VFGM annular plate

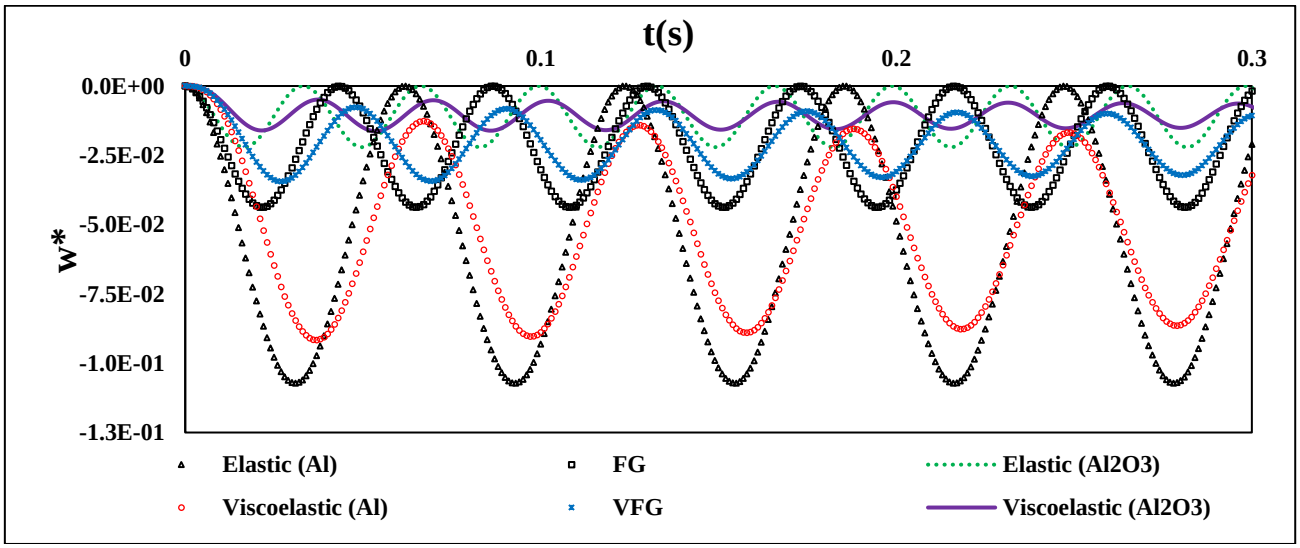

Fig. 15 Transverse response of elastic, FG and VFGM annular plates

In the first numerical example, the transient response due to a step function load is demonstrated. A distributed load as the following is considered

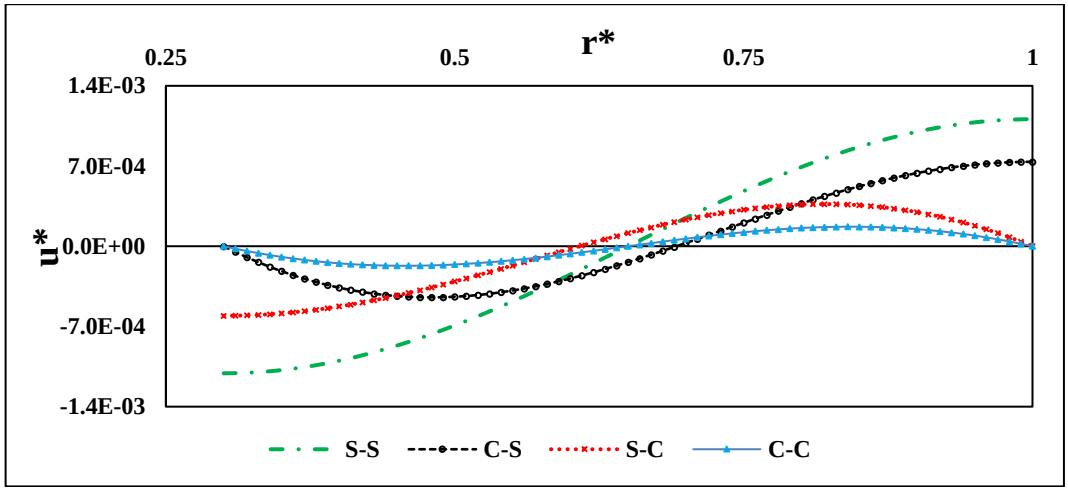

Fig. 16(a) Radial deformed shape for various boundary conditions at (z=h/2, t = 0.5 s)

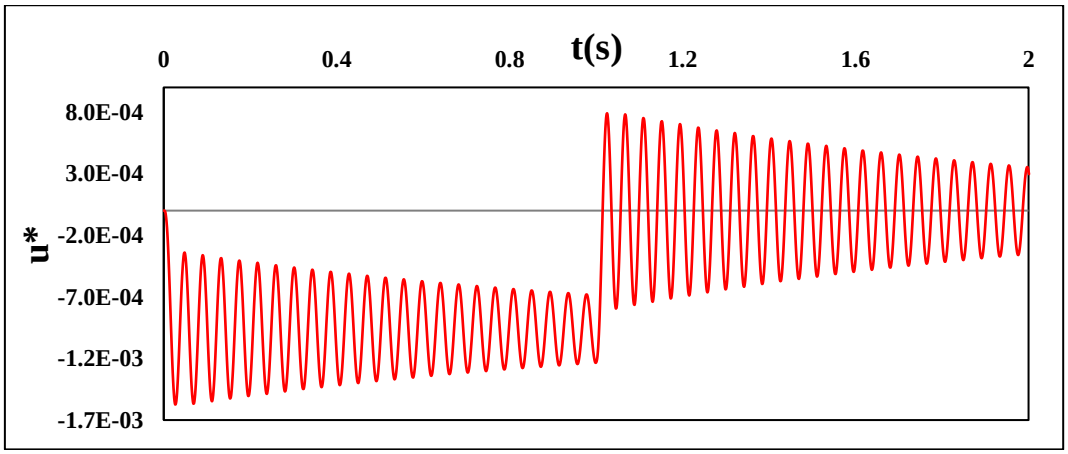

Fig. 16(b) Radial response for step load in time domain(z=h/2)

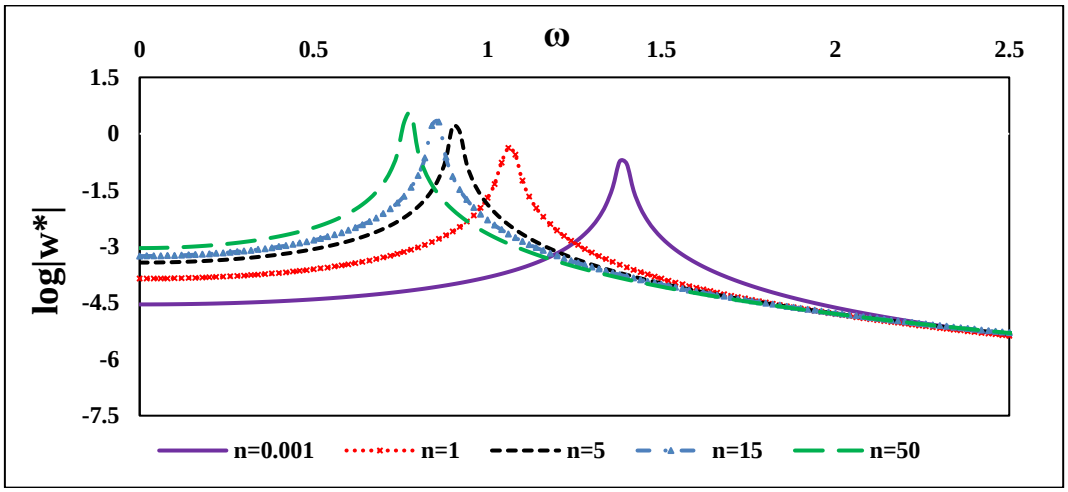

Fig. 17 Dynamic response for different grade index in frequency domain

$$Q(X,T_0) = (1-H(T_0-t_1^*)).Q(X) \quad (25)$$

where $H(t)$ is the Heaviside step function and $t_1^*=t_1/t_0$, t_1=1 sec in this study. The selected spatial parts of the load profile ($Q(X)$) are *constant*, *linear*, *parabolic*, and *sine* distributions. The equations of these profiles have been shown in Table 2. All of the profiles have the same *static equivalent* Q_0=270 Pa.

To demonstrate the accuracy of the current method, analytical results are compared with the FE method. The FSDT and FE results for transverse response at r=(ro+ri)/2

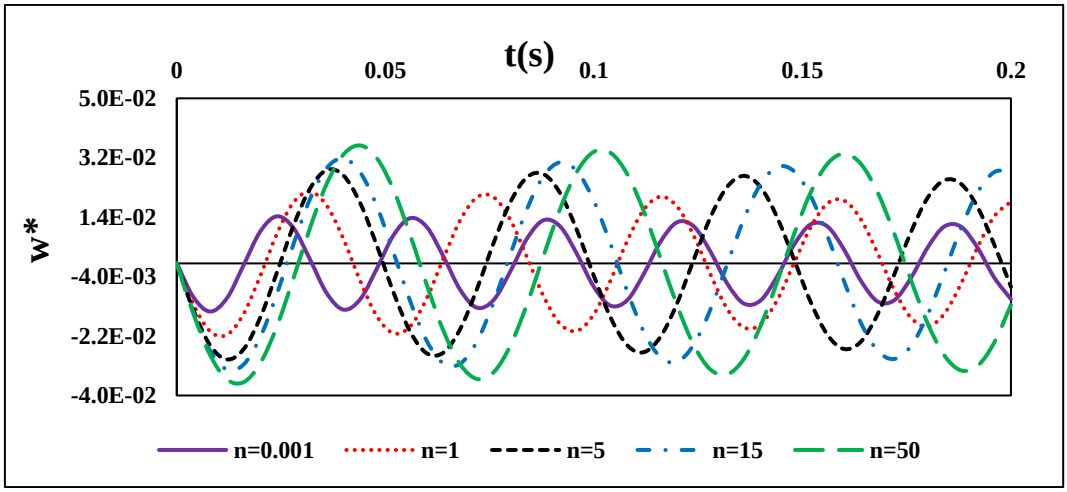

Fig. 18 Transverse response for different grade index in time domain

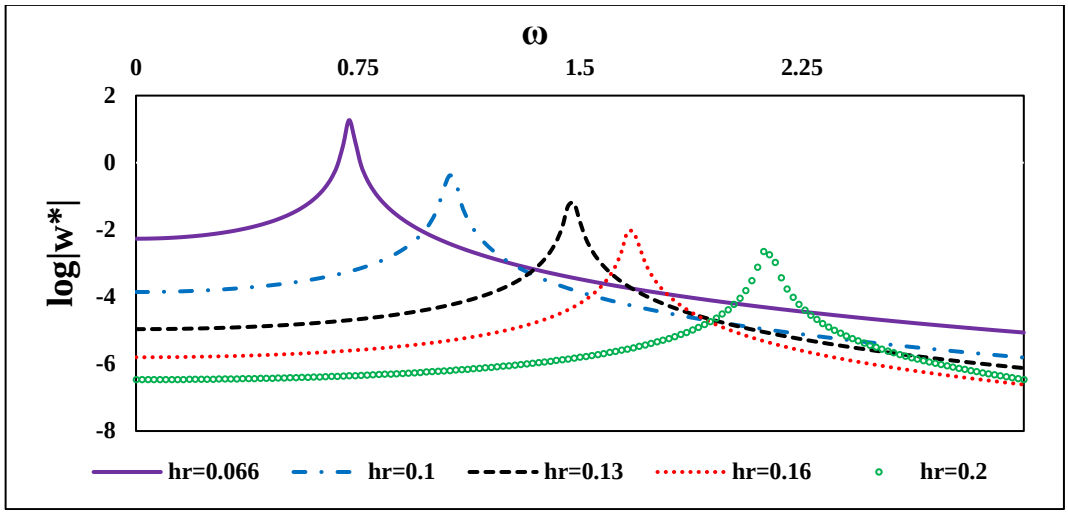

Fig. 19(a) Dynamic response for different thicknesses in frequency domain

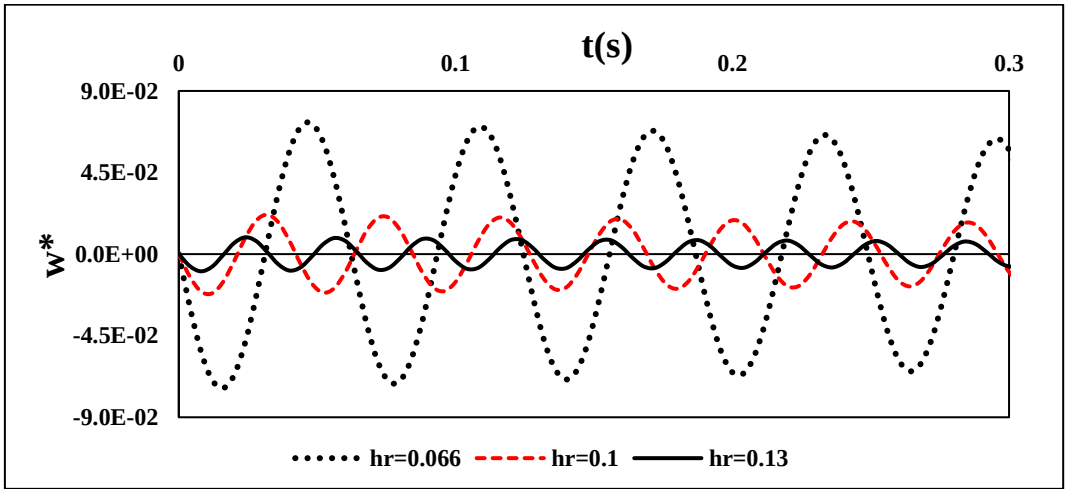

Fig. 19(b) Transverse response for different thicknesses in time domain

have been displayed in Fig. 4. Close matching of the presented results can be recognized from Fig. 4 and difference between the FSDT and FE is insignificant. It should be noted that the computational time for the FE method may be remarkable for a long time but, in the suggested method, this is not important and it possible to find the dynamic response even for a long time immediately. The influences of the FG and VFG materials on the time history for different boundary conditions are given in Figs. 5. The symbols C, S, F stand of Clamped,

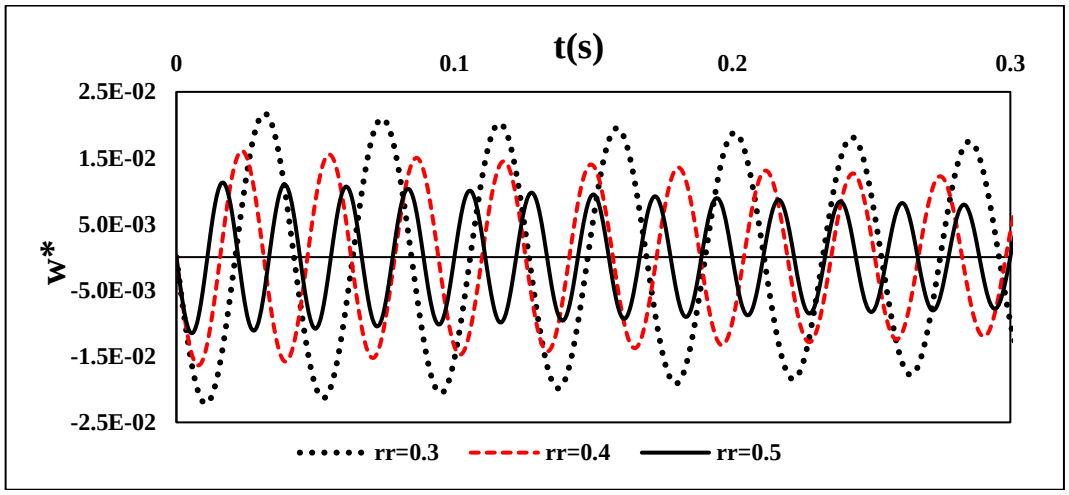

Fig. 20 Transverse response for different radius ratio in time domain

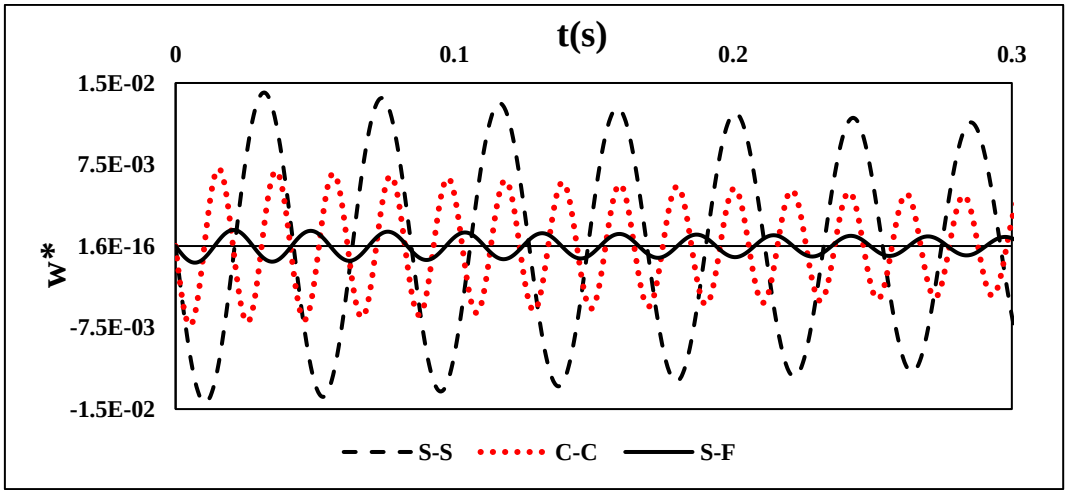

Fig. 21(a) Transverse response for various boundary conditions in time domain

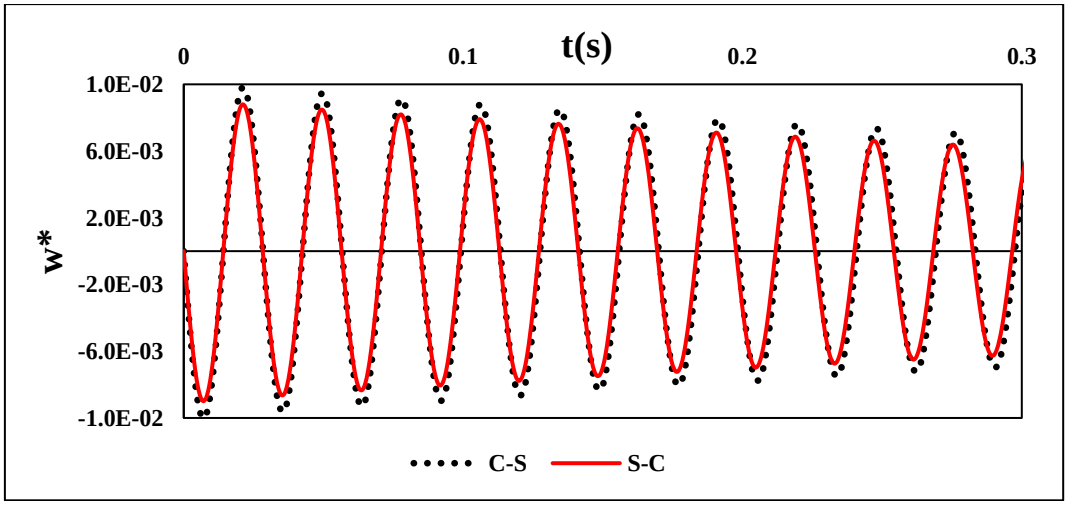

Fig. 21(b) Transverse response for various boundary conditions in time domain

Simple and Free boundary conditions. The boundary conditions are designated with two characters: the first letter denotes the boundary condition at the inner edge and the second shows the outer radius boundary condition e.g., S-F means that the inner radius has simply supported condition and the outer radius is free. Based on Figs. 5, it reveals that the dynamic response of the S-F condition is much less in comparison with another one. In this case (S-F), the first mode of vibrations is rigid body motion, and the reported results for this case relates to the first bending mode

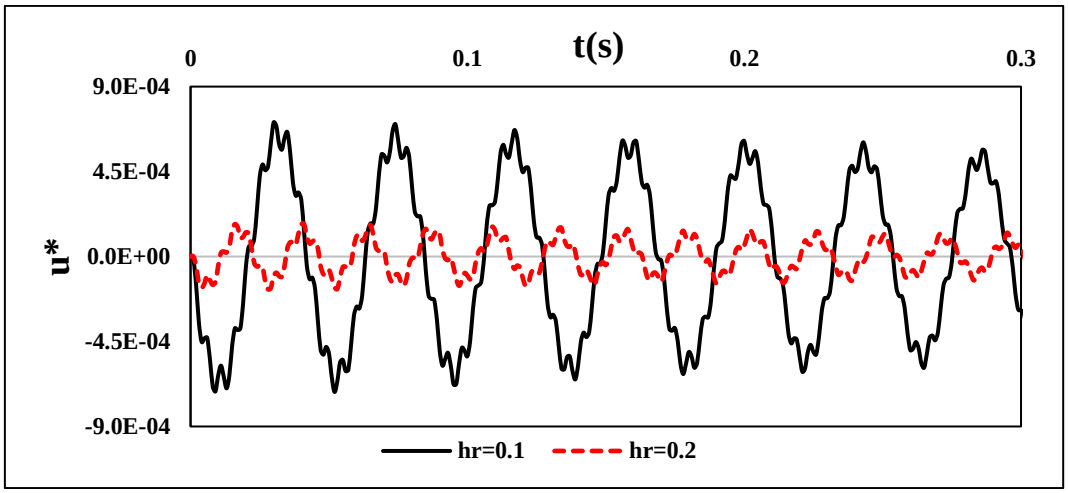

Fig. 22 Radial response for impulse load in time domain (z=h/2)

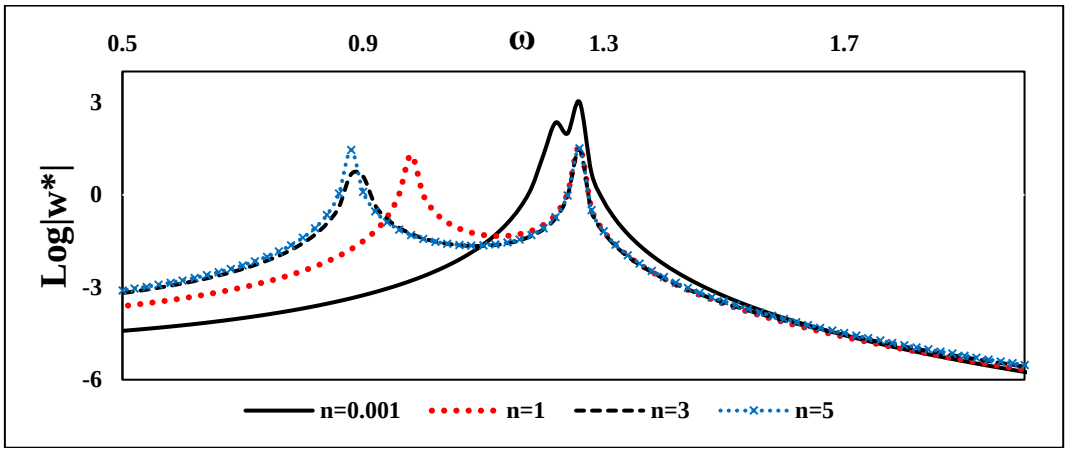

Fig. 23 Transverse response versus different grade index in frequency domain

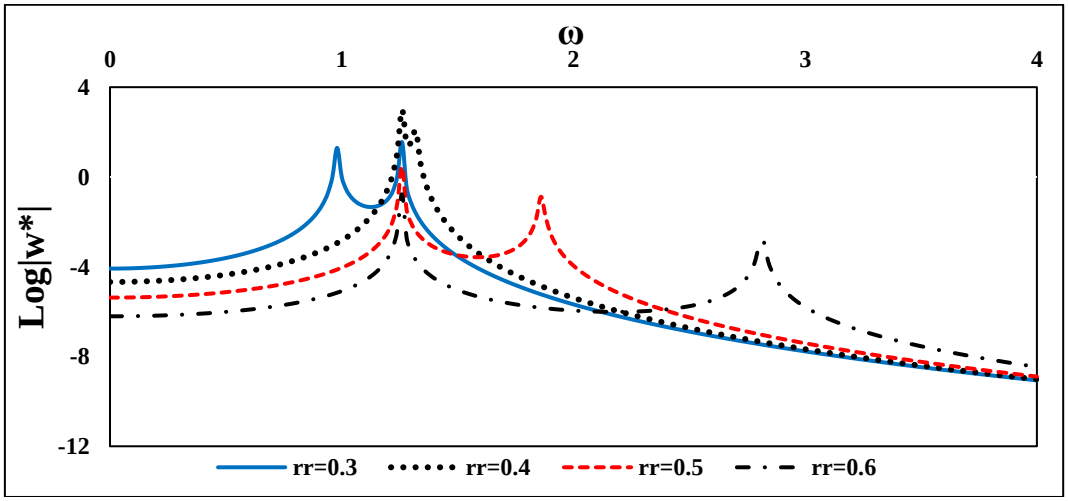

Fig. 24 Transverse response versus radius ratio in the frequency domain

second mode shape). Also, the average values of the transverse deflection for S-S, C-C, S-C, C-S, and S-F boundary conditions are -22.5×10^{-2}, -0.5×10^{-2}, -8×10^{-2}, -9.5×10^{-2} and -0.3×10^{-2}, respectively. In all cases, the viscoelasticity decreases the vibrations amplitude. The effect of various boundary conditions on the transverse deflection for a typical time t = 0.5 s has been shown in Fig. 6. As can be seen, the deformed shapes for S-S boundary conditions is larger than the other cases. The effect of various viscosity coefficients on the time response of VFGM plate has been demonstrated in Fig. 7. It is found that the amplitude and period of dynamic response will

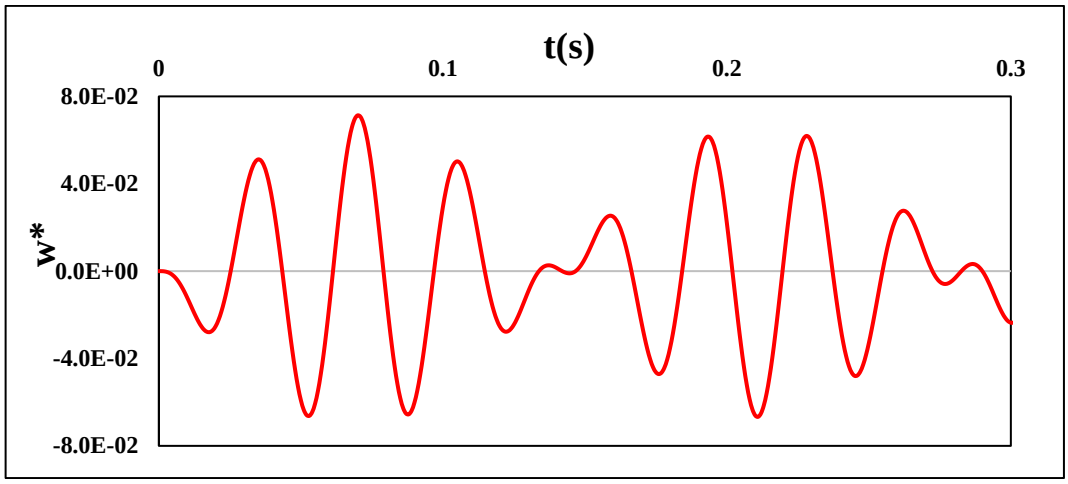

Fig. 25 Transverse response for harmonic load in time domain

decrease by enhancing the values of structural damping due to the dissipation of system energy. The investigations showed that by increasing the viscosity coefficient more than a special value (in this work the value of 7.6E5 Pa.s), this parameter does not affect on the transverse deflection and the oscillations of the system will stop (these figures do not display here). Besides, the calculations showed that by decreasing the viscosity coefficient less than 2.6×10^2 the system exhibits nearly elastic behavior. Fig. 8 visualizes the deformed shapes of the mid-plane under different proposed profiles for a typical time t=0.5 s. The results for constant and linear loadings cases are close. Also, the results for *parabolic* and *sin* cases are nearly the same.

The effects of different elasticity modulus G_1 and G_2 on the lateral response are displayed in Figs. 9. It can be found that by enhancing the value of G_1 the frequency of the response increases and the transverse amplitude reduces but, increasing the value of G_2 leads to enhancing the deflection and period of vibrations. In fact, by increasing G_2, the effect of the Kelvin element in the SLS model decreases and the response of the system depend on the value of G_1.

To survey the convergence of Eqs. (13), the transverse response for one-term and two-term expansions have been illustrated in Fig. 10. It is seen that in the present investigation taking into account, one-term is sufficient for convergence and terms with order-one can help to remove the secularity and finding the dependency of the coefficients on "T_1" ($a_j(T_1)$, $b_j(T_1)$, $c_j(T_1)$ in Eqs. (19)).

In the viscoelastic plate, the oscillations gradually damped with time, due to the structural damping and the system vibrates around its static deflection. The influence of damping on the FSDT transverse response has been shown in Fig. 11. The plate oscillates around its static deflection, and after removing the load, the oscillations of the plate continues around zero. The effect of thickness ratio on the transverse response has been presented in Fig. 12(a) for the FSDT and VFGM plate. By increasing the stiffness due to increasing the plate thickness, the vibrations amplitude decreases and the oscillations frequency increases. Also, the thickness effect on the maximum transverse deflection at a selected position of the VFGM annular plate has been plotted in Fig. 12(b). Based on Fig. 12(b) it can be concluded that the transverse deflection decreases as the plate thickness increases. Fig. 13 demonstrates the effect of different radius ratio on the results. It is seen that by increasing the radius ratio, the amplitude of vibrations decreases and the oscillations frequency increases. It is noted that changing the thickness or radius ratios may alter both the mass and stiffness of the plate.

The effect of grade index on the time history of the midpoint of the plate has been demonstrated in Fig. 14. Increasing the volume fractional exponent increases the period and amplitude response. The influence of various material properties and viscoelasticity on the plate response has been shown in Fig. 15. The results show that the maximum transverse deflection in the VFGM plate is less than the FG plate but in viewpoint of response amplitude, the viscoelastic amplitude is less than the others.

Figs. 16 demonstrate the radially deformed shape under various boundary conditions. As may be observed in Fig. 16a, deflection for C-C boundary conditions is less than another one as expected. Also, the effect of damping has been shown in Fig. 16(b). According to these figures, the radial deflection is smaller than the transverse one.

5.2 Transient response under Impulse excitation

A shock absorption material should have the capacity to reduce or eliminate oscillations over a large range of frequencies. In the present section, the plate response for an impulse load has been analyzed. An impulse excitation applied on the upper surface of the plate as the following form

$$Q(X,T_0)=Q_0\delta(T_0) \tag{26}$$

Where δ is Dirac function. Figs. 17, 18 display the effect of different grade index (n) on the transverse response of the VFGM plate in frequency and time domains. It is detected that with enhancing the grade index, the frequency of the response decreases and the response amplitude increases or increasing the volume fractional exponent tends to convert the material with more deformation

capacity one.

Figs. 19(a), (b) present the transverse response in frequency and time domains for different values of thickness ratios. Increasing the thickness leads enhancing the response frequency and decreasing the response amplitude of the plate. The effect of different radius ratios on the transverse response in the time domain has been shown in Fig. 20. It can be seen that with increasing the radius ratio, decreases the amplitude of vibrations. Figs. 21 present lateral response of a plate subjected to impulse load with different boundary conditions. Based on these figures, with enhancing the plate stiffness, the amplitude of the lateral response decreases. As mentioned before, the first mode of S-F boundary conditions is rigid body motion and in this research, the second mode (which is the first bending mode) has been considered in Eqs. (15).

The radially time-history response of the VFGM annular plate under impulse loading and C-C boundary conditions depicted in Fig. 22. The radial response is obtained at $z=h/2$ in Eqs. (13). It is evident that the amplitude of the vibrations for thicker plates is less the thinner ones.

5.3 Transient response under harmonic load

Now, the plate response subjected to harmonic lateral load has been investigated. The equations of motion that were in the time domain, transform to the frequency domain and then they are solved. The VFGM annular plate includes simply supported at both edges. The mathematical formulation of this response is as the following

$$Q(X,t) = Q_0 \sin(\omega_{ex} t); \omega_{ex} = 200\,Hz \tag{27}$$

The response curve under harmonic load with four grade indexes (n = 0.001, 1, 3, 5) has been presented in Fig. 23. As can be seen, with increasing the graded index, the frequency of the response decreases. In Fig. 24, the variation of frequency response for different radius ratio has been plotted. Four-value for radius ratio has been considered. It is observed that by raising the radius ratio, the frequency of vibrations increases in the studied range.

Fig. 25 shows the response in the time domain for the harmonic load. The beating phenomenon is seen in the response.

6. Conclusions

In this contribution, an analytical approach based on the perturbation technique combined with the generalized Fourier expansion method has been performed to determine the response of the VFGM annular plates under transverse excitation with the FSDT. This procedure can convert a system with variable coefficients to a system of constant coefficients. By providing an appropriate program, it is achievable to determine the effect of different geometrical, materials and loading parameters on the response rapidly, i.e., it is a convenient method for studying the response sensitivity to input parameters. The formulation can use for different boundary conditions. Some of the points mentioned include:

• A unified dynamic analysis method was introduced for the VFGM annular plates.

• The convergence rate of the presented solution is fast.

• In spite of the numerical method (e.g., FE) the computational time does not depend on the selected time duration.

• The FSDT response is in a good matching with the FE.

• The presented formulation can be utilized for different load profiles in time and space domain.

• In the impulse response, with increasing the grade index, the frequency of the response decreases but the response amplitude increases.

• Increasing the radius ratio decreases the amplitude of vibrations and increases the oscillations frequency.

• By increasing the viscosity coefficient (until to a specified value), the response period and amplitude reduce.

• In among of the boundary conditions C-C, C-S, S-C, S-S, the response amplitude for C-C is less the other cases but the frequency of the response for C-C is more than the other cases.

References

Abaqus User Manual (2013), Hibbitt, Karlsson and Sorensen, Inc.

Alavi, S.H. and Eipakchi, H.R. (2018), "An analytical approach for free vibrations analysis of viscoelastic circular and annular plates using FSDT", *Mech. Adv. Mater. Struct.*, 1-15.

Alipour, M. and Shariyat, M. (2014), "Analytical stress analysis of annular FGM sandwich plates with non-uniform shear and normal tractions, employing a zigzag-elasticity plate theory", *Aerosp. Sci. Technol.*, **32**(1), 235-259.

Ansari, R., Gholami, R., Shojaei, M.F., Mohammadi, V. and Sahmani, S. (2014), "Bending, buckling and free vibration analysis of size-dependent functionally graded circular/annular microplates based on the modified strain gradient elasticity theory", *Eur. J. Mech. A-Sol.*, **49**, 251-267.

Barrett, R. (2012), "On the relative position of twist and shear centers in the orthotropic and fiberwise homogeneous Saint-Venant beam theory", *Int. J. Sol. Struct.*, **49**(21), 3038-3046.

Barretta, R. and Elast, J. (2013), "On cesàro-volterra method in orthotropic saint-venant neam", *J. Elast.*, **112**(2), 233-253.

Barretta, R., Feo, L., Luciano, R., Sciarra, F. and Penna, R. (2016), "Functionally graded Timoshenko nanobeams: A novel nonlocal gradient formulation", *Compo.. Part B*, **100**, 208-219.

Brinson, H.F. and Brinson, L.C. (2008), *Polymer Engineering Science and Viscoelasticity; An Introduction*, Springer Science Business Media LLC, U.S.A.

Dai, H.L., Dai, T. and Cheng, S.K. (2015), "Transient response analysis for a circular sandwich plate with an FG central disk", *J. Mech.*, **31**(4), 417-426.

Faghidian, S.A. (2017), "Unified formulations of the shear coefficients in Timoshenko beam theory", *J. Eng. Mech.*, **143**(9), 06017013.

Khadem-Moshir, S., Eipakchi, H.R. and Sohani, F. (2017), "Free vibration behavior of viscoelastic annular plates using first order shear deformation theory", *Struct. Eng. Mech.*, **62**(5), 607-618.

Liang, X., Kou, H., Wang, L., Palmer, A.C., Wang, Z. and Liu, G. (2015), "Three-dimensional transient analysis of functionally graded material annular sector plate under various boundary conditions", *Compos. Struct.*, **132**, 584-596.

Liang, X., Wang, Z., Wang, L. and Liu, G. (2014), "Semi-analytical solution for three-dimensional transient response of functionally graded annular plate on a two parameter

viscoelastic foundation", *J. Sound Vibr*., **333**(12), 2649-2663.
Liang, X., Wang, Z., Wang, L., Izzuddin, B. and Liu, G. (2015), "A semi-analytical method to evaluate the dynamic response of functionally graded plates subjected to underwater shock", *J. Sound J. Sound Vibr*., **336**, 257-274.
Liang, X., Wu, Z., Wang, L. and Liu, G. (2015), "Semianalytical three-dimensional solutions for the transient response of functionally graded material rectangular plates", *J. Eng. Mech*., **141**(9), 1-17.
Malekzadeh, P., Setoodeh, R. and Shojaee, M. (2018), "Vibration of FG-GPLs eccentric annular plates embedded in piezoelectric layers using a transformed differential quadrature method", *Comput. Meth. Appl. M*., **340**, 451-479.
Nayfeh, A.H. (1993), *Introduction to Perturbation Techniques*, John Wiley & Sons, New York, U.S.A.
Pawlus, D. (2016), "Dynamic response control of three-layered annular plate due to various parameters of electrorheological core", *Arch. Mech. Eng*., **63**(1), 74-90.
Rad, B.A. and Shariyat, M. (2016), "Thermo-magneto-elasticity analysis of variable thickness annular FGM plates with asymmetric shear and normal loads and non-uniform elastic foundations", *Arch. Civil Mech. Eng*., **16**(3), 448-466.
Romano, G., Barretta, A. and Barretta, R. (2012), "On torsion and shear of saint-venant beams", *Eur. J. Mech. A-Sol*., **35**, 47-60.
Sadd, M.H. (2009), *Elasticity Theory, Applications and Numeric*, Elsevier Inc., U.S.A.
Salehi, M. and Aghaei, H. (2005), "Dynamic relaxation large deflection analysis of non-axisymmetric circular viscoelastic plates", *Compos. Struct*., **83**(23-24), 1878-1890.
Shariyat, M. and Alipour, M.M. (2013), "A power series solution for vibration and complex modal stress analyses of variable thickness viscoelastic two-directional FGM circular plates on elastic foundations", *Appl. Math. Model*., **37**(5), 3063-3076.
Srividhya, S., Raghu, P., Rajagopal, A. and Reddy, J.N. (2018), "Nonlocal nonlinear analysis of functionally graded plates using third-order shear deformation theory", *Int. J. Eng. Sci*., **125**, 1-22.
Wang, H.J. and Chen, L.W. (2002), "Vibration and damping analysis of a three-layered composite annular plate with a viscoelastic mid-layer", *Compos. Struct*., **58**(4), 563-570.

CC

Acronyms

FGM functionally graded materials

VFGM viscoelastic functionally graded materials

FEM finite elements method

FSDT first order shear deformation theory

SLS standard linear solid

DQ differential quadrature

PDE partial differential equations

Appendix

$$L_{10}[\bullet] = -18e(1+\mu_2)(G_0^*\frac{\partial^2 u_0^*}{\partial T_0^2} + \beta G_1^*\frac{\partial^3 u_0^*}{\partial T_0^3}) + (1+\mu_1)[(24+18G_0^*)\frac{\partial^2 u_0^*}{\partial X^2} + \beta(24+18G_1^*)\frac{\partial^3 u_0^*}{\partial X^2 T_0}] +$$
$$h^*(\mu_1-1)[(4+3G_0^*)\frac{\partial^2 u_1^*}{\partial X^2} + \beta(4+3G_1^*)\frac{\partial^3 u_1^*}{\partial X^2 T_0}];$$
$$L_{20}[\bullet] = -3eh^{*2}G_0^*(1+\mu_2)(G_0^*\frac{\partial^2 u_1^*}{\partial T_0^2} + \beta G_1^*\frac{\partial^3 u_1^*}{\partial T_0^3}) - 36K_s(1+\mu_1)[u_1^* + \beta\frac{\partial u_1^*}{\partial T_0} + \frac{\partial w_0^*}{\partial X} + \beta\frac{\partial^2 w_0^*}{\partial X\,\partial T_0}] +$$
$$h^*(\mu_1-1)[(6G_0^*+8)\frac{\partial^2 u_0^*}{\partial X^2} + \beta(6G_1^*+8)\frac{\partial^3 u_0^*}{\partial X^2 \partial T_0}] + h^{*2}(1+\mu_1)[(3G_0^*+4)\frac{\partial^2 u_1^*}{\partial X^2} + \beta(3G_1^*+4)\frac{\partial^3 u_1^*}{\partial X^2 \partial T_0}];$$
$$L_{30}[\bullet] = -eh^*G_0^*(1+\mu_2)(G_0^*\frac{\partial^2 w_0^*}{\partial T_0^2} + \beta G_1^*\frac{\partial^3 w_0^*}{\partial T_0^3}) - (\mu_1+1)(Q^*G_0^* + \beta G_1^*\frac{\partial Q^*}{\partial T_0}) + K_s h^*(1+\mu_1)(\frac{\partial u_1^*}{\partial X} + \beta\frac{\partial^2 u_1^*}{\partial X\,\partial T_0})$$
$$+K_s h^*(1+\mu_1)(\frac{\partial^2 w_0^*}{\partial X^2} + \beta\frac{\partial^3 w_0^*}{\partial X^2 \partial T_0})$$